33

Quantitative Phase Imaging using Multi-wavelength Optical Phase Unwrapping

Nilanthi Warnasooriya and Myung K. Kim
University of South Florida
U.S.A.

1. Introduction

Quantitative phase imaging is a vital technique in many areas of science. Studying properties and characteristics of biological and other microscopic specimens has been facilitated with new quantitative phase imaging microscopy methods. In quantitative phase imaging, phase images are obtained by interfering two light beams – one reflected from, or traversed through, the specimen and the other reflected from a reference mirror. This can be achieved by two methods; holography or phase-shifting interferometry. In holography, one interferogram is used to produce the phase image, while phase-shifting interferometry uses three or more interferograms.

Each fringe in an interferogram represents an area of data ranging from 0 to 2π . Therefore, the final phase map obtained from a series of interferograms also contains 2π ambiguities. Such phase maps are called 'wrapped' phase maps, and are needed to be 'unwrapped' by removing 2π ambiguities. Once these 2π ambiguities are removed, a continuous surface profile of the test object can be obtained. Such a surface profile provides height information of surface features. Generally, phase unwrapping is done by using numerical algorithms. Most of these numerical algorithms are computationally intensive and can fail when there are irregularities in the test object.

In the basic phase unwrapping method, the phase image is divided to horizontal lines and these lines are unwrapped separately by scanning pixels and adding an offset to each pixel. At each discontinuity a 2π offset is added or subtracted. After all horizontal lines are unwrapped, they are connected vertically and the unwrapping process is done along vertical lines. There are many phase unwrapping methods to remove 2π ambiguities and most can be categorized into two types; path-dependent methods and path-independent methods. Path-dependent methods detect positions of edges and phase ambiguities in images and use this information to calculate phase offset values. In path-independent methods, areas that can cause errors in unwrapping are identified and eliminated before the unwrapping process starts.

In 1994 Ghiglia and Romero used a least squares integration method with phase unwrapping. In this method, which is known as least squares integration of phase gradient method, the phase gradient is obtained as wrapped phase differences along two perpendicular directions and the gradient field is least squares integrated to obtain continuous phase. However, this method is not effective for phase maps with high noise. P.

Source: Advances in Lasers and Electro Optics, Book edited by: Nelson Costa and Adolfo Cartaxo,
ISBN 978-953-307-088-9, pp. 838, April 2010, INTECH, Croatia, downloaded from SCIYO.COM

G. Charette and I. W. Hunter proposed a robust phase unwrapping method for phase images with high noise content. The basic concept behind this method is to identify contiguous areas that are not on or close to a fringe boundary by locally fitting planes to the phase data. Then these areas are phase shifted with respect to one another by multiples of 2π to unwrap the phase.

Software algorithms that exist for detecting and removing 2π ambiguities are mostly computational-intensive and prone to errors when the phase profile is noisy or when the object has irregularities. Multi-wavelength optical phase unwrapping is an easy method that can be used to eliminate 2π ambiguities in phase maps without such problems.

In this chapter we will present quantitative phase images of cells and other microscopic samples, using multi-wavelength optical phase unwrapping. Three types of light sources are used in a standard four-frame phase shifting interferometer to obtain phase profiles with larger beat wavelengths, thus removing 2π ambiguities without increasing phase noise. The effectiveness of multi-wavelength optical phase unwrapping with both incoherent and coherent light sources will be demonstrated.

2. Multi-wavelength optical phase unwrapping

When an object is imaged by a wavelength smaller than the object's height, phase image of the object contains 2π ambiguities as shown in Fig. 1. It is clear that there are many distance values for a given phase value. In order to obtain an unambiguous optical thickness profile, there should be only one z distance for a given phase.

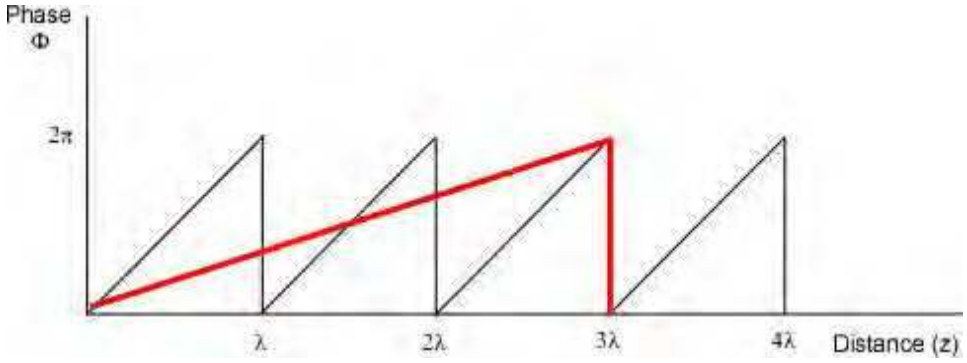

Fig. 1. Phase Vs distance. 2π ambiguities occur when the distance is a multiple of the wavelength. In the axial range Z= 3λ, for a wavelength λ, there are 3 discontinuities (black line), while for a wavelength 3λ, there are no discontinuities (red line).

For years it has been known that a longer wavelength light source produces fewer fringes over a given object than will a short wavelength light source, thus reducing the number of 2π ambiguities in the phase image. However, the drawback is the need of infrared light sources instead of visible light sources. J. C. Wyant has shown that two wavelengths of visible region can be used in the context of holography to produce a longer beat wavelength. Using various pairs of wavelengths from an Argon and HeNe lasers an aspheric optic element was tested. First, a hologram of the test target was obtained by using a wavelength λ_1. Then the hologram was processed and placed at the original position of the

interferometer and illuminated by a second wavelength λ_2. The resultant interferogram was identical to the interferogram that would have been illuminated by a light source of Λ_{12}; the beat wavelength of wavelengths λ_1 and λ_2, where $\Lambda_{12} = \lambda_1\lambda_2 / |\lambda_1 - \lambda_2|$.

The term 'two-wavelength interferometry' was first used by C. Polhemus in a paper where he introduced a two-wavelength technique for interferometric testing. In the method of static interferometry, a fringe pattern obtained with a light source of wavelength λ_1 is recorded and replaced into the system as a moiré reference mask. Then the light source is replaced by one with wavelength λ_2. The resultant moiré fringe pattern is identical to the fringe pattern that would have been obtained with a light source of Λ_{12}. Polhemus modified the method to apply in real time systems. In the method of dynamic interferometry, light sources of λ_1 and λ_2 are operated simultaneously in the interferometer setup, giving a resultant fringe pattern of Λ_{12}.

In 1984, two-wavelength phase shifting interferometry was introduced as an optical phase unwrapping method. In this method, phase shifting interferometry and two-wavelength interferometry were combined to extend the phase measurement range of single-wavelength phase shifting interferometry. Two methods were introduced to solve 2π ambiguities by using two-wavelength phase shifting interferometer. In the first method, two sets of wrapped phase data are obtained with wavelengths λ_1 and λ_2. The data is then used to calculate the phase difference between pixels for beat wavelength Λ_{12}. Then all phase difference values are integrated to calculate the relative surface height of the test object. In the second method, two phase maps of different wavelengths are used to produce a phase map of beat wavelength. The beat wavelength phase map is then used as a reference to correct 2π ambiguities in the single wavelength phase map. Both methods were used to measure 1-D surface heights. Two-wavelength phase shifting interferometry has also been used to obtain three dimensional contour maps of aspheric surfaces with an accuracy of $\Lambda_{12}/100$. However, a disadvantage of this optical phase unwrapping is that the phase noise in each wavelength is magnified by a factor equal to the magnification of the wavelengths. This problem has been addressed by J. Gass, A. Dakoff and M. K. Kim. In the context of digital holography, two phase maps of wavelengths λ_1 and λ_2 are used to produce a phase map called "coarse map" with beat wavelength Λ_{12}. Then one of the single wavelength phase maps is used to reduce the amplified phase noise of the coarse map. The resultant 'fine map' has noise similar to the noise of the single wavelength phase map, with a larger axial range free of 2π ambiguities.

The two-wavelength phase unwrapping method has been extended to multiple wavelengths; enabling measurements of steep surfaces without software phase unwrapping. A hierarchical phase unwrapping algorithm that chooses a minimum number of wavelengths to increase the accuracy of optical unwrapping has been introduced by C. Wagner, W. Osten and S. Seebacher. The basic principle of this method is to start with a larger beat wavelength. Then a systematic reduction of beat wavelengths is used to improve the accuracy of the measurement while the information of the preceding measurements is used to eliminate 2π ambiguities. A similar version of hierarchical phase unwrapping has been presented by U. Schnars and W. Jueptner, however it has not been used experimentally. Three-wavelength phase unwrapping algorithms have been introduced in both interferometry and digital holography enabling measurements of steep surfaces

without software phase unwrapping. While the principle of multi-wavelength phase unwrapping has been known in interferometry, until recently known applications had been confined to optical profilers with raster-scanned point-wise interferometry. Other than recent digital holography experiments, the first known application of multi-wave phase unwrapping to full-frame phase images in interferometry has been presented by N. Warnasooriya and M. K. Kim.

2.1 Principle of two-wavelength optical phase unwrapping

The basis of multi-wavelength optical phase unwrapping method is the idea of beat wavelength. For two wavelengths λ_1 and λ_2, the beat wavelength Λ_{12} is defined by

$$\Lambda_{12} = \frac{\lambda_1 \lambda_2}{|\lambda_1 - \lambda_2|} \tag{1}$$

For the m^{th} wavelength λ_m, the surface profile Z_m of an object is related to the phase difference φ_m as follows;

$$Z_m = \frac{\lambda_m \varphi_m}{2\pi} \tag{2}$$

It is apparent that unambiguous range of Z can be increased by using a longer λ.

Consider two single wavelength phase maps φ_1 and φ_2 with wavelengths λ_1 = 530 nm and λ_2 = 470 nm respectively. The beat wavelength Λ_{12} for λ_1 and λ_2 is Λ_{12} = 4.151 μm. The Λ_{12} can be increased by choosing closer values of λ_1 and λ_2. The phase map for Λ_{12} is obtained by subtracting one single wavelength phase map from the other and then adding 2π whenever the resultant value is less than zero. This phase map is called "coarse map" φ_{12}. The surface profile for coarse map φ_{12} is given by $Z_m = \Lambda_{12}\varphi_{12}/2\pi$. However, the phase noise in each single wavelength phase map is magnified by the same factor as the magnification of wavelengths. In the two-wavelength optical phase unwrapping method introduced by J. Gass *et.al.*, the phase noise is reduced by using the following steps.

First, the surface profile Z_{12} is divided into integer multiples of a single wavelength, say λ_1. Then, the result is added to the single wavelength surface profile Z_1. This significantly reduces the phase noise in the coarse map. However, at the boundaries of wavelength intervals λ_1 the noise of the single wavelength phase map appears as spikes. These spikes can be removed by comparing the result with the coarse map surface profile Z_{12}. If the difference is more than half of λ_1, addition or subtraction of one λ_1 depending on the sign of the difference removes the spikes. The final result 'fine map' has a noise level equal to that of single wavelength surface profile. If a single wavelength phase map φ_m contains a phase noise of $2\pi\varepsilon_m$ the two-wavelength phase unwrapping method works properly for $\varepsilon_m < \lambda_m / 4\Lambda_{12}$. Using a lager beat wavelength reduces the maximum noise limit.

2.2 Principle of three-wavelength optical phase unwrapping

The advantage of three wavelength phase unwrapping method is that the beat wavelength can be increased without reducing the maximum noise limit. Suppose the three chosen wavelengths are λ_1 = 625 nm, λ_2 = 590 nm, and λ_3 = 530 nm. The first two wavelengths give beat wavelength Λ_{12} = 10.53 μm. Instead of using the surface profile of Z_{12}, which has

a high noise, an identical surface profile can be produced by using surface profiles Z_{13} and Z_{23} with beat wavelengths Λ_{13} = 3.49 μm and Λ_{23} = 5.21 μm. The resultant "coarse map of coarse maps" φ_{13-23} with surface profile Z_{13-23} also has the same beat wavelength $\Lambda_{13-23} = \Lambda_{13}\Lambda_{23} / |\Lambda_{13} - \Lambda_{23}| = 10.53$ μm.
The noise reduction is done as follows. In the first step, the quantity of integer multiples of Λ_{13} present in the range Z_{13-23} is calculated. The result $Z(a)$ is given by

$$Z(a) = \text{int}\left[\frac{Z_{13-23}}{\Lambda_{13}}\right]\Lambda_{13} \tag{3}$$

In the next step, the result is added to the surface profile Z_{13}.

$$Z(b) = Z(a) + Z_{13} \tag{4}$$

The resultant map is then compared with Z_{13-23}. If the difference $Z(c)$ is more than half of Λ_{13}, one Λ_{13} is added or subtracted depending on the sign difference.

$$Z(d) = \begin{cases} Z(c) + \Lambda_{13} & \text{if } Z(c) > \Lambda_{13}/2 \\ Z(c) & \text{if } -\Lambda_{13}/2 \le Z(c) \le \Lambda_{13}/2 \\ Z(c) - \Lambda_{13} & \text{if } Z(c) < -\Lambda_{13}/2 \end{cases} \tag{5}$$

The resultant surface profile $Z(d)$ is called "intermediate fine map" and has significantly reduced noise. Any remaining noise is due to the noise in the phase map φ_{13}. The remaining noise in $Z(d)$ is reduced by using a single wavelength, say λ_1. First, the intermediate fine map $Z(d)$ is divided into integer multiples of λ_1.

$$Z(e) = \text{int}\left[\frac{Z(d)}{\lambda_1}\right]\lambda_1 \tag{6}$$

Then the result is added to the single wavelength surface profile Z_1.

$$Z(f) = Z(e) + Z_1 \tag{7}$$

The resultant map $Z(f)$ is then compared with Z_1. If the difference is more than half of λ_1, one λ_1 is added or subtracted depending on the sign difference. The noise in the final map is equal to the noise in the single wavelength surface profile Z_1. The maximum noise level ε_m in the single wavelength phase map for the three wavelength phase unwrapping to work is given by the smaller value of $\Lambda_{13}/4\Lambda_{12} \sim 8.3\%$ or $\lambda_1/4\Lambda_{13} \sim 4.5\%$. Therefore, the three wavelength phase unwrapping method increases the beat wavelength without magnifying the noise in the final phase map.
The method can be applied to phase images obtained with any type of light source, regardless of the coherence length of the source.

3. Multi-wavelength optical phase unwrapping experiments

In this experiment, four step phase shifting algorithm is applied to the interference microscope. Though the minimum number of intensity values needed for phase calculation

is three, even a small error in measurements can cause a large phase error. Taking four intensity measurements can reduce this effect. In order to acquire phase images, the Michelson interferometer is used as the experimental setup as shown in Figure (2).

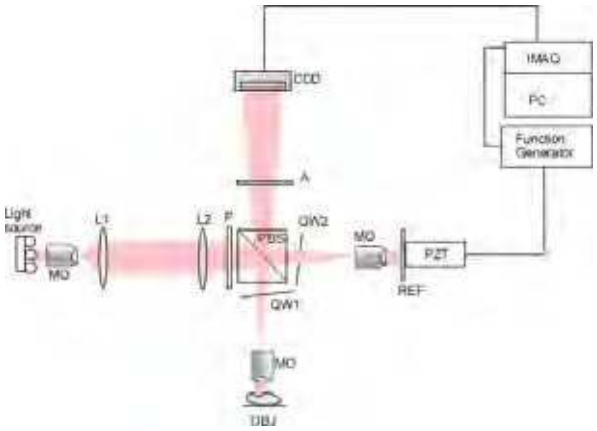

Fig. 2. A schematic diagram of the experimental setup. See text for details.

The light is expanded and collimated by the microsocpe objective MO and the lens L1, respectively. The light is then linealry polarized by the polarizer P. The polarized beam splitter (PBS) splits the incoming beam into an S-polarized (polarization plane is perpendicular to polarization axis) ray and a P-polarized (polarization plane is parallel to polarization axis) ray. The S-polarized beam is reflected at the PBS to illuminate the sample object OBJ and the P-polarized beam is transmitted throught the PBS to illuminate the reference mirror REF. When the S-polarized light passes through the quarter wave plate (QW1), the phase changes by 90° and it becomes circulary polarized. After reflcting at the mirror and going through another 90° phase shift at QW1, the light becomes P-polarized. This change from S-polarization to P-polarization avoids light traveling back to the light source and directs all reflected light to the charge-coupled device (CCD). Similarly, P-polarized light illuminating the REF changes to S-polarized light and travels to the CCD. At the analyzer A, the two S-polarized and P-polarized light beams are changed into a common polarization state so that the interference can occur on the CCD plane.

The polarizer-analyzer pair also controls the variation of the realtive intensity between the two arms. The reference mirror is mounted on a piezo-electric transducer (PZT). A function generator supplies a ramp signal to the PZT to dither the reference mirror by a distance of one wavelength. Images are recorded at quarter wavelength intervals.

Images acquired by the CCD are sent to an image acquisition board (National Instruments IMAQ PCI-1407) installed in the computer. The Intensity $I(x,y)$ of the light captured by CCD can be written as;

$$I(x,y) = I_O(x,y) + I_B(x,y) + I_R(x,y) + 2\sqrt{I_O(x,y)I_R(x,y)}\cos\left[\phi_i + \phi(x,y)\right] \tag{8}$$

Here $I_O(x,y)$ is the part of the beam reflected by the object that is coherent with respect to $I_R(x,y)$, the intensity of the beam reflected by the reference mirror. $I_B(x,y)$ is part of reflection from the object that is incoherent with respect to the reference – i.e. outside the

coherence length. $\phi(x,y)$ the relative phase between the object and the reference mirror and ϕ_i is the phase shift introduced by moving the reference mirror by quarter wavelength intervals. Intensity distributions corresponding to the four images, acquired at $\phi_i = 0, \pi/2, \pi$ and $3\pi/2$, can be given as follows;

$$\begin{aligned} I_0 &= I_O + I_B + I_R + 2\sqrt{I_O I_R}\cos\phi \\ I_{\pi/2} &= I_O + I_B + I_R - 2\sqrt{I_O I_R}\sin\phi \\ I_\pi &= I_O + I_B + I_R - 2\sqrt{I_O I_R}\cos\phi \\ I_{3\pi/2} &= I_O + I_B + I_R + 2\sqrt{I_O I_R}\sin\phi \end{aligned} \tag{9}$$

The phase map of the object is given by;

$$\phi = Tan^{-1}\left(\frac{I_{3\pi/2} - I_{\pi/2}}{I_0 - I_\pi}\right) \tag{10}$$

Once a phase profile of the specimen is obtained, it can be used to determine the height profile of the specimen.
The optical path difference (OPD) between the object wave and reference wave is given by

$$OPD = \frac{\lambda\phi}{2\pi} \tag{11}$$

Here λ is the wavelength of the light beam and ϕ is the relative phase between the object and reference mirror. In the given Michelson type interferometer, the height profile of the object is half the OPD because the light travels towards the object, reflects and travels back. Therefore, the height profile h is related to the phase ϕ s follows.

$$h = \frac{1}{2}\left(\frac{\lambda}{2\pi}\right)\phi \tag{12}$$

4. Multi-wavelength optical phase unwrapping using light emitting diodes

Experimental results of multi-wavelength optical phase unwrapping using light emitting diodes (LED) are presented below. In interferometry, LEDs have been used as light sources in order to reduce the speckle noise inherent to lasers. Since LEDs have coherence lengths in micron range, speckle noise is greatly reduced. All the LEDs used in the experiment are Luxeon™ Emitter diodes from Lumileds Lighting LLC and have a Lambertian (high dome) radiation pattern. The peak wavelength, luminous flux, calculated and measured coherence lengths for red, red-orange, amber and green LEDs used in this experiment are shown in the Table 1. The calculated coherence length of a light source is given by $l_c = (2\ln 2/\pi)(\overline{\lambda^2}/\Delta\lambda)$, where $\overline{\lambda}$ is the mean wavelength and $\Delta\lambda$ is the full width half maximum (FWHM) of Gaussian spectrum. The coherence length was directly measured here by counting the number of fringes in the interference pattern of the tilted mirror object.

Colour	Luminous Flux Φ (lm) *	Peak Wavelength λ (nm)	Spectral Width (nm)	Calculated Coherence Length (μm)	Measured Coherence Length (μm)
Red	44	653.83±0.07	27.24±0.15	6.91±0.04	9.15±2.45
Red-Orange	55	643.42±0.07	23.21±0.14	7.85±0.05	10.29±2.57
Amber	36	603.48±0.03	17.53±0.05	9.14±0.03	10.86±2.56
Green	25	550.18±0.09	38.39±0.19	3.42±0.02	3.85±1.46

Table 1. Characteristics of LEDs. Luminous flux values are at 350 mA, Junction Temperature T_J= 25°C. * LuxeonTM Emitter and Star sample information AB11, 2 (Feb 2002).

4.1 Results for two-wavelength optical phase unwrapping

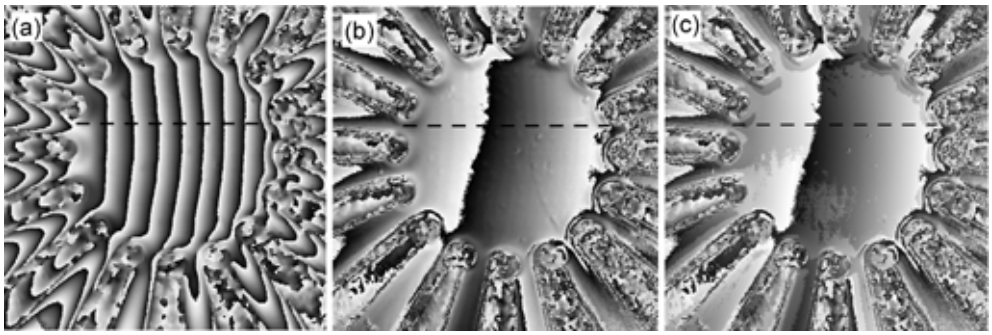

Fig. 3. Results of two-wavelength optical phase unwrapping. (a) a single wavelength phase map; (b) two-wavelength coarse map; (c) two-wavelength fine map with reduced noise.

The object here in the Fig. 3 is a micro-electrode array biosensor. It consists of 16 gold electrodes on a Pyrex glass substrate. The center is a 125 μm diameter circle with an approximate thickness of 2 μm. The center of the device was imaged and the experimental results for two wavelength optical phase unwrapping are shown in Fig. 3. Red (λ_1 = 653.83 nm) and green (λ_2 = 550.18 nm) LEDs are used as the two wavelengths. The beat wavelength Λ_{12} = 3.47 μm. Images are of a 184 μm × 184 μm area. Fig. 3(a) shows a single wavelength phase map φ_1 with λ_1 = 653.83 nm. The coarse map φ_{12} with Λ_{12} = 3.47 μm is shown in Fig. 3(b) and the final phase map with the reduced noise is shown in Fig. 3(c). Figure 4 shows cross section profiles of phase maps along the lines shown in Fig. 3 and the phase noise in the chosen regions. Figure 4(a) is a cross section of the single wavelength phase map with λ_1 = 653.83 nm and Fig. 4(b) is a cross section of coarse map with Λ_{12} = 3.47 μm. A cross section of the fine map with reduced phase noise is shown in Fig. 4(c). For maps (a), (b) and (c), the vertical axis is 4 μm. The root mean square (RMS) noise of the coarse map is 43.27 nm. This is shown in Fig. 4(d). Figure 4(e) shows the reduced noise in the fine phase map. Since the center of the device has a curvature, a paraboloid is fitted to the data. The red dotted line is the best-fit parabolic curve. After subtracting the curvature from the data, the Fig. 4(f) shows the corrected phase noise of 10.29 nm.

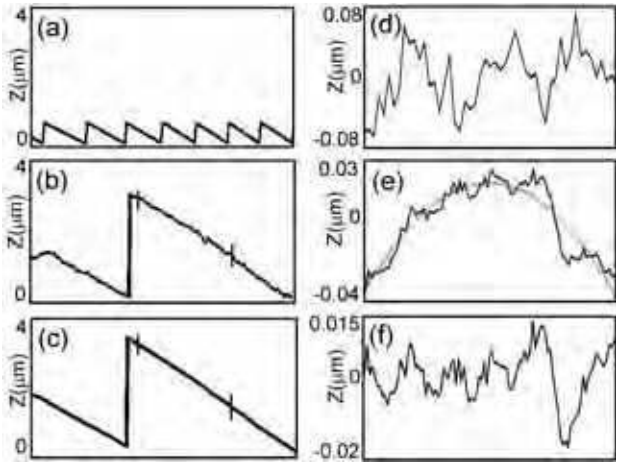

Fig. 4. Surface profiles for two-wavelength optical phase unwrapping. (a) single wavelength surface profile; (b) surface profile of coarse map; (c) surface profile of final unwrapped phase map with reduced noise; (d) noise of the coarse map in the region between the two markers in plot (b). RMS noise is 43.27 nm; (e) noise of final unwrapped phase map in the area shown in (c). Red dotted line is the best fit parabolic curvature and black solid line is data; (f) corrected phase noise of the unwrapped phase map, after subtracting the curvature of the object. RMS noise is 10.29 nm.

4.2 Results for three-wavelength optical phase unwrapping

The experimental results for three-wavelength optical phase unwrapping are presented in Fig. 5. Red (λ_1 = 653.83 nm), amber (λ_2 = 603.48 nm) and green (λ_3 = 550.18 nm) are used as the three wavelengths. The beat wavelength Λ_{13-23} = 7.84 μm. The object is the same micro-electrode array biosensor used in the previous section. Images are of a 184 μm × 184 μm area. Figure 5(a) is the single wavelength phase map φ_1 with λ_1 = 653.83 nm. The three wavelength coarse map is shown in Fig. 5(b) with a beat wavelength Λ_{13-23} = 7.84 μm. The final phase map with the reduced noise is shown in Fig. 5(c).

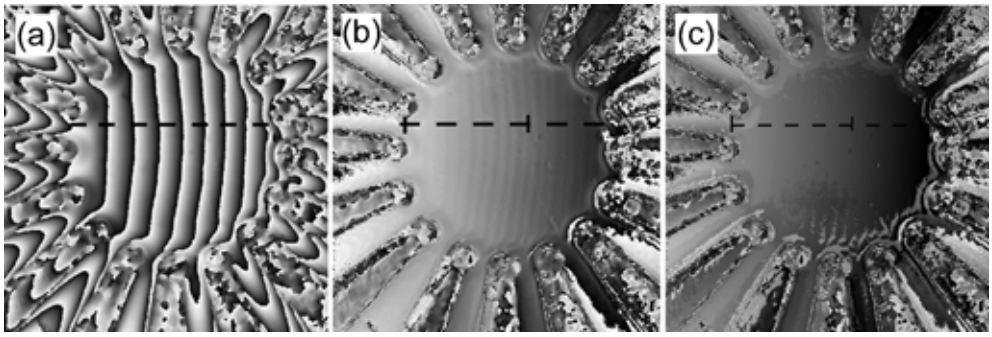

Fig. 5. Results of three-wavelength optical phase unwrapping. (a) single wavelength phase map; (b) three-wavelength coarse map; (c) three-wavelength fine map with reduced noise.

Cross section profile of each phase map is taken along the lines shown in Fig. 5. These cross section profiles and phase noise of coarse and fine maps are shown in Fig. 6. Figures 6 (a)-6(c) show surface profiles of single wavelength phase map, coarse map and fine map respectively. The vertical axis is 11 μm. Figure 6(d) shows 105.79 nm RMS noise of the coarse map. Because of the curvature of the object surface, a paraboloid is fitted with the final fine map data as shown in Fig. 6(e). The black line is data and the red dotted line shows the best-fit parabolic curve. Corrected phase noise in the final fine map is 4.78 nm, which is shown in Fig. 6(f).

The comparison of the two-wavelength optical phase unwrapping method to the three-wavelength optical phase unwrapping method shows that the three-wavelength phase unwrapping increases the axial range of the object, without increasing phase noise. These results show that the two-wavelength phase unwrapping method produced a 3.47 μm unambiguous range with 10.29 nm phase noise, while the three-wavelength phase unwrapping method produced much larger 7.48 μm unambiguous range with smaller 4.78 nm phase noise.

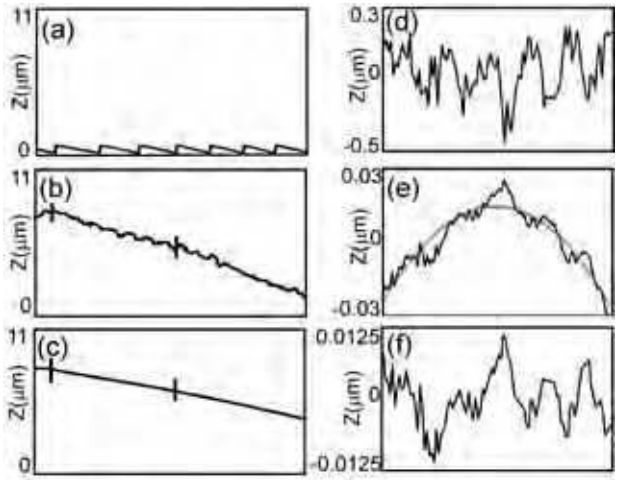

Fig. 6. Surface profiles for three-wavelength optical phase unwrapping. (a) single wavelength surface profile; (b) surface profile of coarse map; (c) surface profile of final unwrapped phase map with reduced noise; (d) noise of the coarse map in the region between the two markers in plot (b). RMS noise is 105.79 nm; (e) noise of final unwrapped phase ma in the area shown in (c). Red dotted line is the best fit parabolic curvature and black solid like is data; (f) corrected phase noise of the unwrapped phase map, after subtracting the curvature of the object. RMS noise is 4.78 nm.

Multi-wavelength optical phase unwrapping methods can also be used for biological cells as shown in Fig. 7. Here, Fig. 7 shows a single wavelength phase map, a coarse map and a fine map of onion cells using red (653.83 nm), amber (603.48 nm) and green (550.18 nm) wavelengths. The beat wavelength is 7.48 μm. Image size is 184 μm × 184 μm. The final fine map clearly shows the cell walls by eliminating the 2π ambiguities that would exist in a single wavelength phase image.

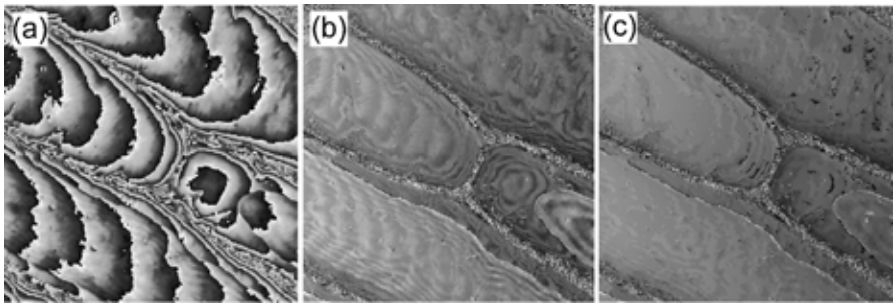

Fig. 7. Results of three-wavelength optical phase unwrapping. (a) a single wavelength phase map; (b) three-wavelength coarse map; (c) three-wavelength fine map with reduced noise.

5. Three-wavelength optical phase unwrapping using laser diodes & lasers

In the previous section, incoherent light sources (light emitting diodes) were used to reduce the speckle noise inherent in lasers. However, light emitting diodes are available in only several different wavelengths. Therefore, wavelength combinations that produce large beat wavelengths are limited. Because of small coherence lengths of light emitting diodes, imaging phase profiles of samples with features larger than the coherence range is not possible. In this section, the effectiveness of the three-wavelength optical phase unwrapping method is tested by using laser diodes and a ring dye laser. Laser diodes have been frequently used as a light source in interferometry due to their frequency tunability, smaller size and cost, compared to those of lasers. They also have shorter coherence lengths, typically few centimeters, compared to coherence length of lasers. However, laser diodes also have a limited availability of wavelength choices. Using a ring dye laser, the beat wavelength can be extended to more than a hundred micrometers. In this section, the effectiveness of the optical phase unwrapping method with any type of light source is presented. The results of three-wavelength optical phase unwrapping using laser diodes are shown in Fig. 8 and the results obtained with a ring dye laser as the light source are shown in Fig. 9, Fig. 10 and Fig. 11.

Figure 8 shows experimental results of three-wavelength optical phase unwrapping method using laser diodes. The object here is a micro-electrode array biosensor with 16 gold electrodes on a Pyrex glass substrate. The three wavelengths are λ_1 = 677.81 nm, λ_2 = 639.37 nm and λ_3 = 636.89.81 nm with a beat wavelength of Λ_{13-23} = 11.27 μm. Figure 8(a) is the single wavelength phase map with λ_1 = 677.81 nm. The three-wavelength coarse map is shown in Fig. 8 (b). The final fine map with reduced noise is show in Fig. 8 (c), and the 3-D rendering in Fig. 8 (d). The unwrapped phase map shows the grainy surface of electrodes.

In Fig. 9, results show phase images of a sample of cheek cells (basal mucosa) illuminated with a ring dye laser. The sample is illuminated by using wavelengths λ_1 = 579 nm, λ_2 = 577 nm and λ_3 = 574 nm. The beat wavelength is 167 μm. The image size is 102 μm per side. Here, Fig. 9(a) is the direct image of the cheek cell. Figure 9(b) shows the single wavelength phase map obtained using λ_1 = 579 nm. The coarse map produced by the three wavelengths is shown in Fig. 9(c). The final fine map with reduced noise is shown in Fig. 9(d) and the 3-D rendering of the final fine map is shown in Fig. 9(e).

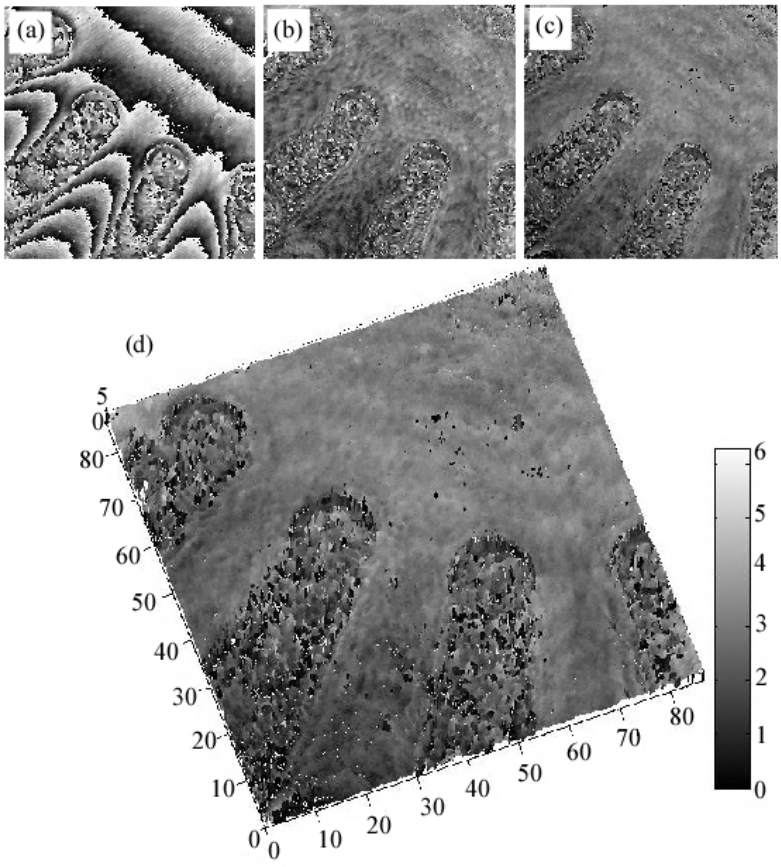

Fig. 8. Three-wavelength optical phase unwrapping of the biosensor using laser diodes. Image size is 86.6 μm per side. (a) a single wavelength phase map with λ_1 = 677.81 nm; (b) three-wavelength coarse map with Λ_{13-23} = 11.27 μm; (c) three-wavelength fine map with reduced noise; (d) 3-D rendering of (c).

In Fig. 10 and Fig. 11, the sample is a piece of 33 1/3 rpm long playing (LP) record. For 33 1/3 rpm records the typical width at the top of the groove ranges from 25.4 μm to 76.2 μm and the groove depth is ~15 μm. The sample is coated with a layer of 200 nm aluminum for better reflectivity. The three wavelengths used for the optical phase unwrapping process is λ_1 = 577 nm, λ_2 = 575 nm and λ_3 = 570 nm, with a beat wavelength of 166 μm. Figure 10(a) is the single wavelength phase map with λ_1 = 577 nm. The three-wavelength coarse map is shown in Fig. 10(b) with beat wavelength Λ_{13-23} = 166 μm. The bottom of the grooves

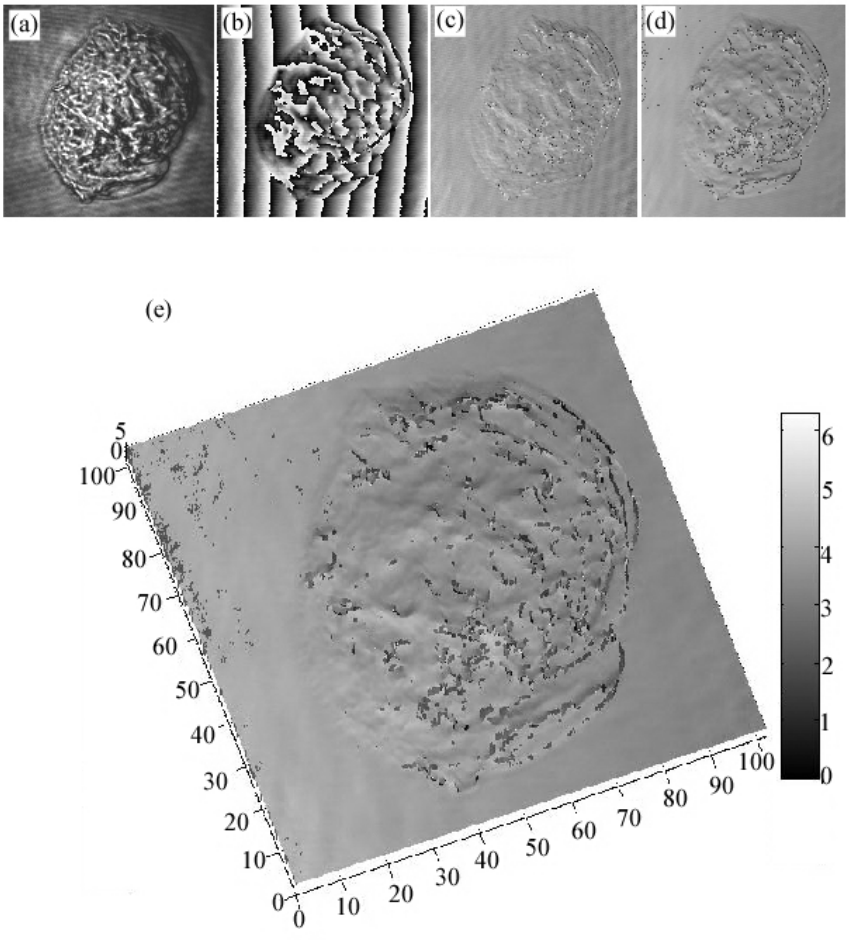

Fig. 9. Three-wavelength optical phase unwrapping of cheek cells using ring dye laser. Image size is 103 μm per side. (a) direct image of the cheek cell; (b) a single wavelength phase map; (c) three-wavelength coarse map; (d) three-wavelength fine map with reduced noise; (e) 3-D rendering of (d).

appears in darker color. The final fine map with reduced noise is shown in Fig. 10(c). Figure 10(d) is the 3-D rendering of the final fine map. In the final unwrapped phase map, the width of the top of the groove is measured along the line shown in Fig. 4(d). The measured width is 44 μm.

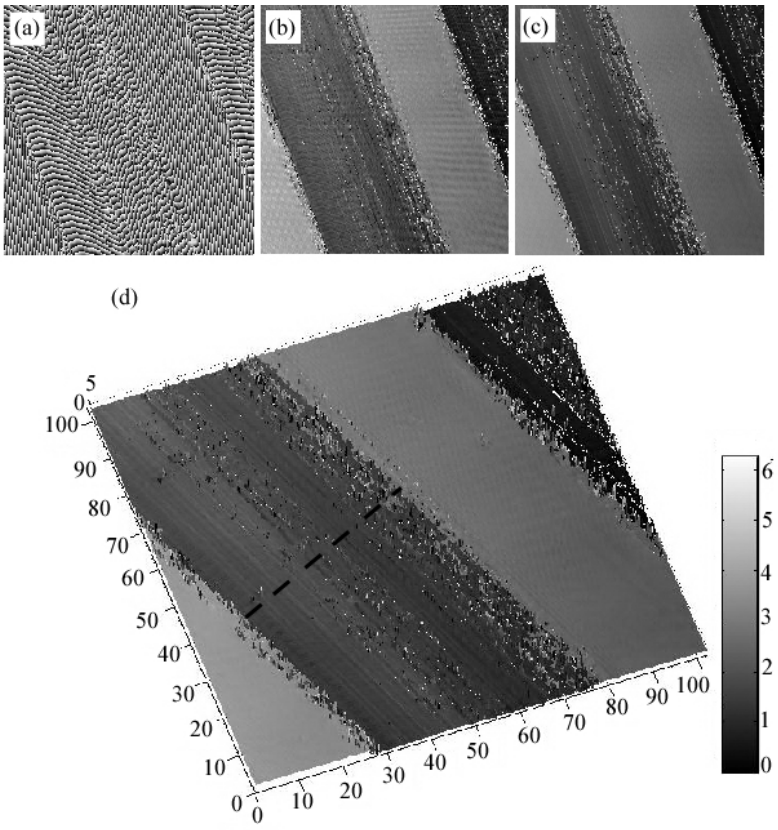

Fig. 10. Three-wavelength optical phase unwrapping of LP record grooves. Image size is 102 μm per side; (a) a single wavelength phase map; (b) three-wavelength coarse map; (c) three-wavelength fine map with reduced noise; (d) 3-D rendering of (c). The grove width is 44 μm.

Cross-sections and phase noise of the coarse and fine maps are shown in Fig.11. Figure 11(a) is the unwrapped coarse map and Fig. 11(b) is the final fine map with reduced noise. Figure 11(c) is the surface profile of the coarse map along the line shown in Fig. 11(a). The RMS noise in the coarse map in the area shown is 2.12 μm and this is shown in Fig. 11(d). Figure 11(e) shows the surface profile of fine map along the line shown in Fig. 11 (b). The groove depth h = 18 μm.

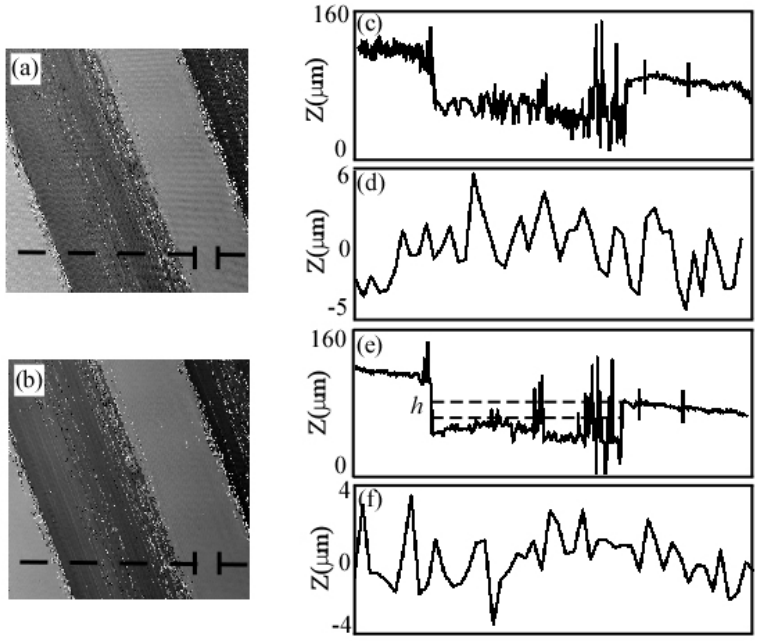

Fig. 11. Surface profiles of LP record grooves. (a) three-wavelength coarse map, (b) three-wavelength fine map with reduced noise, (c) surface profile of coarse map along the line shown in (a); (d) noise in coarse map in the area shown in (a). RMS noise is 2.12 μm ; (e) surface profile of fine map along the line shown in (b). The groove depth h = 18 μm ; (f) noise in the fine map in the area shown in (b). RMS noise is 1.36 μm.

5. Summary

In summary, this chpater demonstrates the effectiveness of the multi-wavelength optical unwrapping method. To our knowledge this is the first time that three wavelengths have been used in interferometry for phase unwrapping without increasing phase noise. Unlike conventional software phase unwrapping methods that fail when there is high phase noise and when there are irregularities in the object, the multi-wavelength optical phase unwrapping method can be used with any type of object. Software phase unwrapping algorithms can take more than ten minutes to unwrap phase images. This is a disadvantage when one needs to study live samples in real time or near – real time. The multi-wavelength optical unwrapping method is significantly faster than software algorithms and can be effectively used to study live samples in real time. Another advantage is that the

optical phase unwrapping method is free of complex algorithms and needs less user intervention.

The method is a useful tool for determining optical thickness profiles of various microscopic samples, biological specimens and optical components. The optical phase unwrapping method can be further improved by adding more wavelengths, thus obtaining beat wavelengths tailored for specific samples.

6. References

Charette, P. G.; Hunter, I. W. (1996). Robust phase-unwrapping method for phase images with high noise content. *Applied Optics*, Vol. 35, Issue 19, (July 1996), pp. 3506-3513, ISSN 0003-6935.

Cheng, Y; Wyant, J. C. (1984). Two-wavelength phase shifting interferometry. *Applied Optics*, Vol. 23, Issue 24, (December 1984), pp. 4539-4543, ISSN 0003-6935.

Cheng, Y.; Wyant, J. C. (1985). Multiple-wavelength phase-shifting interferometry. *Applied Optics*, Vol. 24, Issue 6, (March 1985), pp. 804-807, ISSN 0003-6935.

Creath, K.; Cheng, Y.; Wyant, J. C. (1985). Contouring aspheric surfaces using two-wavelength phase-shifting interferometry. *Journal of Modern Optics*, Vol. 32, No. 12, (December 1985), pp. 1455-1464, ISSN 0950-0340.

Dilhaire,S.; Grauby, S.; Jorez, S.; Lopez, L. D. P.; Rampnoux, J.; Claeys, W. (2002). Surface displacement imaging by interferometry with a light emitting diode. *Applied Optics*, Vol. 41, Issue 24, pp.4996-5001, (August 2002),ISSN 0003-6935.

De Groot, P.; Kishner, S. (1991). Synthetic wavelength stabilization for two color laser-diode interferometry. *Applied Optics*, Vol. 30, Issue 28, pp 4026-4033 (October 1991), ISSN 0003-6935.

Fedeyev, V.; Haber, C. C. (2003). Reconstrcution of mechanically recorded sound by image processing. *LBNL Report 51983*, 2003.

Fercher, A.; Drexler, W.; Hitzenberger, C. K.; Lasser, T. (2003). Optical coherence tomography - principles and applications. *Reports on Progress in Physics*, Vol. 66, pp. 239-303 (January 2003).

Gass, J.; Dakoff, A.; Kim, M. K. (2003). Phase imaging without 2π ambiguity by multiwavelength digital holography. *Optics Letters*, Vol. 28, Issue 13, (July 2003), pp. 1141-1143, ISSN 0146-9592.

Ghiglia,D. C.; Romero, L. A. (1994). Robust two-dimensional weighted and unweighted phase unwrapping that uses fast transforms and iterative methods. *Journal of the Optical Society of America A*, Vol. 11, No. 1, (January 1994), pp. 107-117, ISSN 1084-7529.

Ishii, Y.; Onodera, R. (1995). Phase-extraction algorithm in laser-diode phase shifting interferometry. *Optics Letters*, Vol. 20, Issue 18, pp. 1883-1885 (September 1995), ISSN 0146-9592.

Liu, J.; Yamaguchi, I. (2000). Surface profilometry with laser-diode optical feedback interferometer outside optical benches. *Applied Optics*, Vol. 39, Issue 1, pp. 104-107 (January 2000), ISSN 0003-6935.

Lukashkin,A. N.; Bashtanov, M. E.; Russell, I. J. (2005). A self-mixing laser diode interferometer for measuring basilar membrane vibrations without opening the

cochlea. *Journal of Neuroscience Methods*, Vol. 148, Issue 2, pp. 122-129 (October 2005), ISSN 0735-7044.

LuxeonTM Emitter and Star sample information AB11, 2 (Feb 2002).

Meiners-Hagen, K.; Burgarth, V.; Abou-Zeid, A. (2004). Profilometry with a multi-wavelength diode laser interferometer. *Measurement Science & Technology*, Vol. 15, No. 4, (April 2004), pp. 741-746, ISSN 0957-0233.

Montfort, F.; Colomb, C.; Charriere, F.; Kuhn, J.; Marquet, P.; Cuche, E.; Herminjard, S.; Depeursinge, C. (2006). Submicrometer optical tomography by multi-wavelength digital holographic microscopy. *Applied Optics*, Vol. 45, Issue 32, (November 2006), pp. 8209-8217, ISSN 0003-6935.

Onodera, R.; Ishii, Y. (1996). Phase-extraction analysis of laser-diode phase shifting interferometry that is insensitive to changes in laser power. *Journal of the Optical Society of America A*, Vol. 13, Issue 1, pp. 139-146 (January 1996), ISSN 1084-7529.

Parshall, D; Kim, M. K. (2006). Digital holographic microscopy with dual wavelength phase unwrapping. *Applied Optics*, Vol. 45, Issue 3, (January 2006), pp. 451-459, ISSN 0003-6935.

Polhemus,C. (1973). Two-wavelength interferometry. *Applied Optics*, Vol. 12, Issue 9, (September 1973), pp. 2071-2074, ISSN 0003-6935.

Repetto, L.; Piano, E.; Pontiggia, C. (2004). Lensless digital holographic microscope with light-emitting diode illumination. *Optics Letters*, Vol. 29, Issue 10, pp. 1132-1134 (May 2004), ISSN 0146-9592.

Schnars, U; Jueptner, W. (2005). *Digital Holography – Digital Hologram Recording, Numerical Reconstruction, and Related Techniques*, Springer, ISBN 354021934X, Berlin Heidelberg.

Servin, M.; Marroquin, J. L.; Malacara, D; Cuevas, F. J. (1998). Phase unwrapping with a regularized phase-tracking system. *Applied Optics*, Vol. 37, No. 10, (April 1998), pp. 1917-1923, ISSN 0003-6935.

Tziraki, M.; Jones, R.; French, P. M. W.; Melloch, M. R.; Nolte, D. D. (2000). Photorefractive holography for imaging through turbid media using low coherent light. *Applied Physics B*, Vol. 70, No. 1, (January 2000), pp. 151-154, ISSN 0946-2171.

Wagner, C.; Osten, W.; Seebacher, S. (2000). Direct shape measurements by digital wavefront reconstruction and multiwavelength countoutring. *Optical Engineering*, Vol. 39, Issue 1, (January 2000), pp. 79-85, ISSN 0091-3286.

Warnasooriya, N.; Kim, M. K. (2006). Multi-wavelength Phase Imaging Interference Microscopy. *Proceedings of SPIE – Volume 6090 Three-Dimensional and Multidimensional Microscopy: Image Acquisition and Processing XIII*, pp. 60900U-1 - 60900U-8, SPIE, January 2006, San Jose, California, USA.

Warnasooriya, N.; Kim, M. K. (2007). LED-based multi-wavelength phase imaging interference microscopy. *Optics Express*, Vol. 15, Issue 15, (July 2007), pp. 9239-9247, ISSN 1094-4087.

Warnasooriya, N.; Kim, M. K. (2009). Quantitative phase imaging using three-wavelength optical phase unwrapping, *Journal of Modern Optics*, Vol. 56, No. 1, (January 2009), pp; 85-92, ISSN 0950-0340.

Wyant,J. C. (1971). Testing aspherics using two-wavelength holography. *Applied Optics*, Vol. 10, Issue 9, (September 1971), pp. 2113-2118, ISSN 0003-6935.

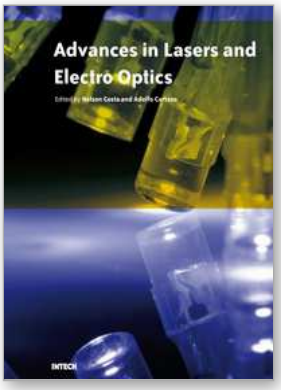

Advances in Lasers and Electro Optics

Edited by Nelson Costa and Adolfo Cartaxo

ISBN 978-953-307-088-9
Hard cover, 838 pages
Publisher InTech
Published online 01, April, 2010
Published in print edition April, 2010

Lasers and electro-optics is a field of research leading to constant breakthroughs. Indeed, tremendous advances have occurred in optical components and systems since the invention of laser in the late 50s, with applications in almost every imaginable field of science including control, astronomy, medicine, communications, measurements, etc. If we focus on lasers, for example, we find applications in quite different areas. We find lasers, for instance, in industry, emitting power level of several tens of kilowatts for welding and cutting; in medical applications, emitting power levels from few milliwatt to tens of Watt for various types of surgeries; and in optical fibre telecommunication systems, emitting power levels of the order of one milliwatt. This book is divided in four sections. The book presents several physical effects and properties of materials used in lasers and electro-optics in the first chapter and, in the three remaining chapters, applications of lasers and electro-optics in three different areas are presented.

InTech Europe
University Campus STeP Ri
Slavka Krautzeka 83/A
51000 Rijeka, Croatia
Phone: +385 (51) 770 447
Fax: +385 (51) 686 166
www.intechopen.com

InTech China
Unit 405, Office Block, Hotel Equatorial Shanghai
No.65, Yan An Road (West), Shanghai, 200040, China
中国上海市延安西路65号上海国际贵都大饭店办公楼405单元
Phone: +86-21-62489820
Fax: +86-21-62489821